SPIE 6068, temp: 101–111 (2006) (Electronic Imaging 2006) 19 Jan 2006 LBNL-59227

Quantum efficiency characterization of LBNL CCD's Part 1: the Quantum Efficiency Machine

Donald E. Groom, Christopher J. Bebek, Maximilian Fabricius, Armin Karcher, William F. Kolbe, Natalie A. Roe, and Jens Steckert

Lawrence Berkeley National Laboratory, Berkeley CA 94720

ABSTRACT

Instrumentation was developed in 2004 and 2005 to measure the quantum efficiency of the Lawrence Berkeley National Lab (LBNL) total-depletion CCD's, intended for astronomy and space applications. This paper describes the basic instrument. Although it is conventional even to the parts list, there are important innovations. A xenon arc light source was chosen for its high blue/UV and low red/IR output as compared with a tungsten light. Intensity stabilization has been difficult, but since only flux ratios matter this is not critical. Between the light source and an Oriel MS257 monochromator are a shutter and two filter wheels. High-bandpass and low-bandpass filter pairs isolate the 150-nm wide bands appropriate to the wavelength, thus minimizing scattered light and providing order blocking. Light from the auxiliary port enters a 20-inch optical sphere, and the 4-inch output port is at right angles to the input port. An 80 cm drift space produces near-uniform illumination on the CCD. Next to the cold CCD inside the horizontal dewar is a calibrated reference photodiode which is regulated to the PD calibration temperature, 25° C. The ratio of the CCD and in-dewar reference PD signals provides the QE measurement. Additional cross-calibration to a PD on the integrating sphere permits lower-intensity exposures.

Keywords: CCD's, quantum efficiency, detectors, astronomy, instrumentation

1. INTRODUCTION

Totally-depleted thick p-channel charge-coupled devices (CCD's) have been developed over the past decade in the MicroSystems Lab at the Lawrence Berkeley National Laboratory (LBNL).[1] In the first years, all of our characterization was done at the UCO/Lick Observatory Detector Development Laboratory in Santa Cruz, CA. With the ramp-up of activity on the SuperNova Acceleration Probe (SNAP),[3] substantial effort has gone into characterization at LBNL. The quantum-efficiency (QE) workbench (The Quantum Efficiency Machine) described here is part of that effort.

The design goals were for an automatic computer-controlled quantum efficiency measurement of a 6 cm × 6 cm CCD over a 300 nm–1200 nm spectral range. Results should be reproducible, and have a relative error of less than 1% and an absolute error of less than 3%. We hope for a smaller absolute error.

Since the internal QE of the CCD's is nearly 100% over a wide spectral range, a measurement of the reflectivity R is a necessary compliment. In this region, QE $= 1 - R$, but in general QE $\leq 1 - R$. The instrument to make this measurement is the subject of the following paper.[4] It is inside the "dark box" of the QE Machine during measurements, making use of light from the axial port of the monochromator via an optical fiber bundle. Alternatively, the fiber bundle goes to a spot projector used to measure the CCD point spread function (PSF). This instrument is also placed inside the dark box when direct QE measurements are not in progress.

Constructing and debugging this instrument was Jens Steckert's Diplom thesis project (FH Karlsruhe) under the LBNL supervision of A. Karcher. His thesis[2] provides details only summarized here.

Further author information:
Send correspondence to D. Groom at DEGroom@lbl.gov
J. Stekert's present address: Fachhochschule Karlsruhe, Germany

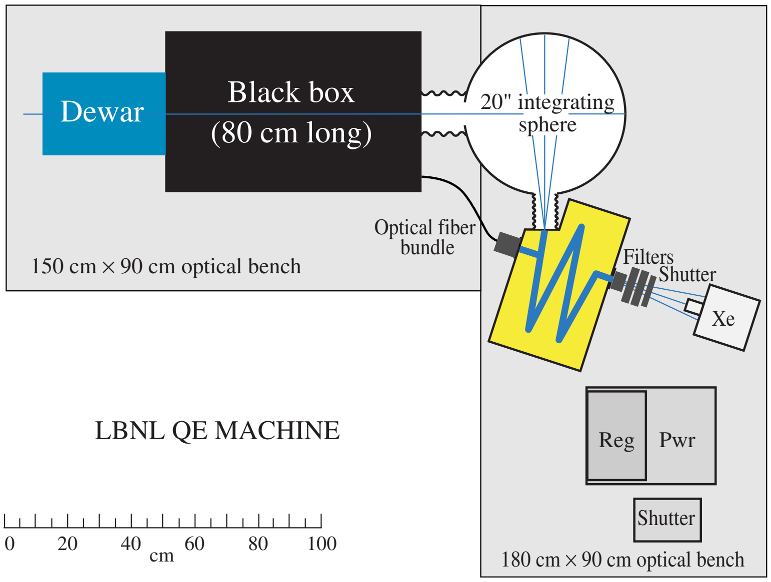

Figure 1. Plan view of the QE Machine

2. INSTRUMENTATION

A plan view of the QE Machine is shown in Fig. 1, and a picture of it in Fig. 2. It consists of a Xe arc light source (with an intensity controller), a shutter with a reflective face, two filter wheels, an 0.5 m monochromator with two exit ports, a 20-in diameter integrating sphere with the main output port at 90° to the input port, a dark box so that the dewar window is about 1 m from the integrating sphere exit port, a large-aperture shutter in front of the dewar window, and finally the dewar containing the CCD and the calibrated reference PD. The reference PD in the dewar is temperature-controlled to its calibration temperature, 25° C. A more detailed list of parts is given in Appendix A.

The 90° bend was chosen because of lab space restrictions. The assembly is mounted on two Newport optical tables, 90 cm × 150 cm and 90 cm × 180 cm, which are clamped together.

2.1. Light source

A 100 W Xe arc light source was chosen for its high blue/near ultraviolet (UV) output and low infrared (IR) output as compared with a quartz/halogen source. The broadened emission lines can be 30 times more intense than the nearby average intensity, but since in all cases it is only the ratio of CCD charge to integrated reference PD current which matters, these intensity spikes are not an issue.

It was originally planned that the Uniblitz VS25 shutter between the light source collimator and the filter wheels would control exposure times. In practice, it is open during an entire scan, but protects the filters and monochromator from continuous exposure to the fairly high-power collimated beam during other beam-on times. Its highly reflective blades on the light source side prevent excessive heating. Its double-overlapped blades provide very high light suppression. It opens/closes in 3 ms.

For the CCD a number proportional to the integrated charge during an exposure is obtained, while a possibly time-varying current is provided by the reference PD. The (Keithley 6485) picoammeter measures the current average over its sampling time, then is dead for an equal time before repeating. An average of these samples over the shutter-open multiplied by the exposure time is a good estimator of the total charge integral for the PD. The picoammeter has minimum noise at its longest sampling time (1 s), but a 0.5 s sampling time is normally used to minimize “edge effects” in the measurement.

While results obtained in this way are relatively independent of light intensity variations, an intensity controller was thought to be advisable. Feedback is provided by a light-sensing head, a small temperature-controlled

Figure 2. CCD image of the QE Machine

PD which is designed to mount on a light-housing port at right angles to the collimated beam. This does not work very well, apparently through some combination of arc movement and heating/extra intensity because of light reflected back from the shutter or filter stack. Illuminating the sensor head via a beam splitter in front of the shutter also failed because of reflected light and possibly heating. Since the settling time of the controller is about 15 s, it could not stabilize during the shutter-open time. However, the stabilization works quite well if the feedback PD is mounted on one of the small ports on the integrating sphere.

At present the large-aperture shutter in front of the dewar is used for exposure control. The scan sequence will be described below.

2.2. Filter wheels

Between the shutter and the monochromator entrance port are two motorized filter wheels with five openings each. These are operated by the monochromator controller. Since each must have one open position, at most eight positions can contain filters. Ideally, these would define eight 100-nm bandpasses which cover the spectral range 200–1200 nm; these would eliminate 2nd order light (blue contamination at the red end) and help minimize scattered light. In practice such filters are not available, so most positions are occupied by two dichroic filters, one short-bandpass and one long-bandpass, which define an overlapping series of ~ 150 nm bandpasses. Two glass bandpass filters are used at the blue end, and a single long-pass filter turning on at 950 nm is at the red end. The bandpasses are indicated in Fig. 3. The minimal overlap at 370 nm is unfortunate, but this causes little problem. A list of the filters is given in Appendix A (Table A2.)

2.3. Monochromator

After calculations of the possible impact of scattered light, it was decided to use a single monochromator rather than the double monochromator chosen by the ESO group.[5] (The 150-nm bandpass filters further reduce concerns about scattered light.) A half-meter rather than quarter-meter monochromator was chosen mostly because other groups used and thought highly of the Oriel MS-257.

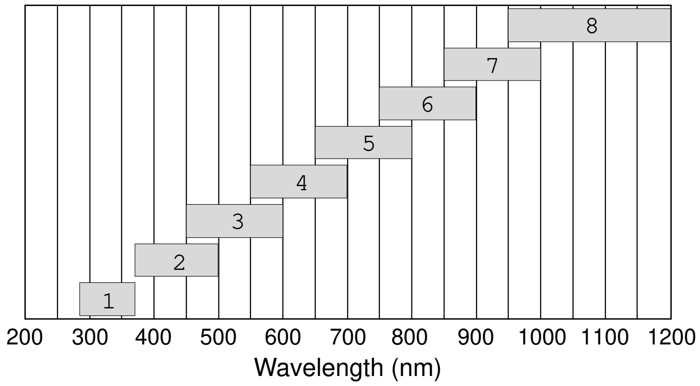

Figure 3. Approximate bandpasses of the filter stacks.

Two 1200 lines/mm gratings are used, one with a 350 nm blaze and the other with a 750 nm blaze. With these two gratings the desired range of wavelengths (350–1100 nm) can be covered with never less than 50% efficiency. A planar mirror is mounted on a third grating turret position so that a "white light" throughput can be obtained.

Motor-driven slits are mounted on the input and axial output ports, and a 3.2-mm fixed slit is mounted on the lateral output port. Light from the axial port goes to the integrating sphere. Alternatively, the light can be directed to the lateral port, which is coupled via an optical fiber bundle going to the dark box. The maximum motor-drive slit width is 2 mm, corresponding to $\Delta\lambda = 6.4$ nm. For the 3.2 mm fixed slit it is about 10 nm. Light intensity on the CCD is changed by changing the slit widths. The widths are the same to minimize $\Delta\lambda$.

2.4. Integrating sphere

The 20-inch diameter LabSphere integrating sphere has a 2-inch entrance port, a 4-inch exit port at right angles to the entrance port, and two 1-inch ports for monitor PD's. One is presently occupied, and the current recorded during measurements in the same way the current is recorded for the standard PD in the dewar.

The figure of merit for an integrating sphere is the fraction of its area covered by ports, and the manufacturer suggests $\leq 5\%$ for good uniformity at an output port. A very conservative 1% was chosen, dictating the large sphere. In retrospect this was hardly necessary; a 12-inch or even smaller sphere would have been adequate.

The dewar window is about 100 cm from the integrating sphere exit port. The intensity near the window was scanned horizontally and vertically with a 1 cm^2 PD, with the results shown in Fig. 4. The slight difference between the horizontal and vertical scans is not significant. A fit yielded the inexplicable $\cos^{4.46}\theta$ radial dependence shown by the solid line in the plot. The intensity has fallen by 1% at a radius of 6 cm, and data corrections are easily made.

2.5. Dark box

The 82 cm long $\times$ 61 cm square wooden dark box visible in Fig. 2 provides a "drift space" between the integrating sphere exit port and the CCD to obtain a more uniform CCD illumination. It also houses removable apparatus such as the reflectometer and the spot projector used for point-spread function (PSF) measurements. A series of removable baffles prevents secondary light scattered by the nearly-black interior from reaching the CCD. Part of the top and the side of the box nearest the user is hinged and can be lifted upward for access, as can be seen in the figure. The seal between the door and the rest of the box consists of mating black tongue-and-groove strips which mesh to form a light-tight labyrinth.

The bottom is open, so that the optical table is available for mounting other instrumentation inside the box. Small aluminum "bulkheads" are easily fitted with feedthrough connectors to provide dark connections to such instruments.

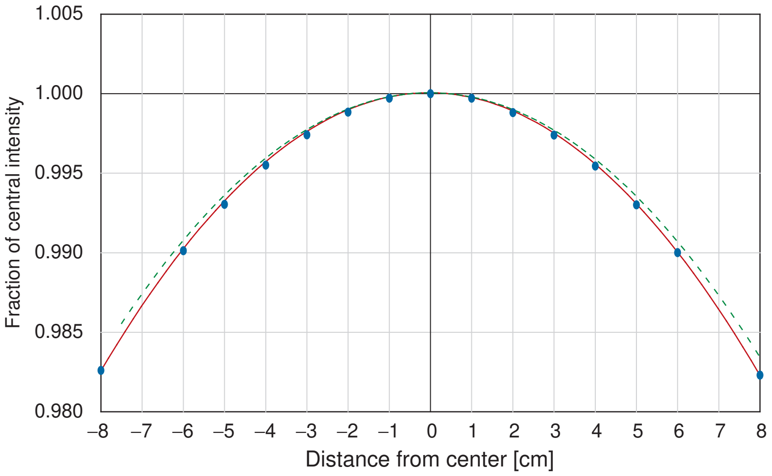

Figure 4. Position dependence of light intensity in front of the dewar, as obtained by scanning with a photodiode. Measurements are shown by the circles. The solid curve is a fit to $\cos^n \theta$, where θ is the angle between the center of the integrating sphere and the photodiode. The fitted value is $n = 4.46$. The dashed curve is from a less-dependable vertical scan.

Figure 5. Test CCD and coplanar calibrated photodiode in the dewar, as seen from the dark box through the large-aperture shutter. The photodiode is temperature-stabilized at 25° C, while the CCD is near 130 K.

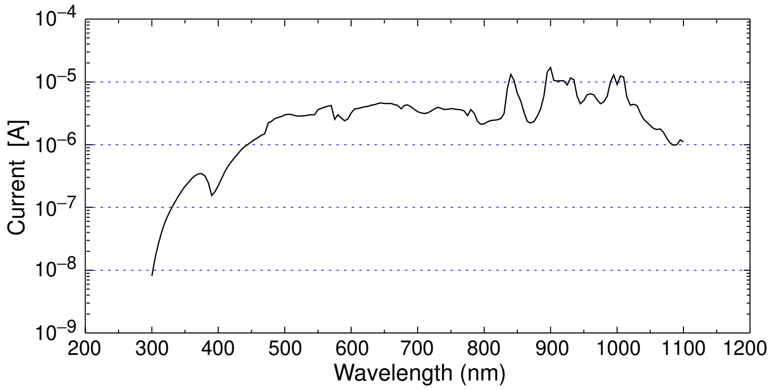

Figure 6. Current in a 1 cm^2 photodiode in the dewar as a function of wavelength, with a 10 nm bandpass beam from the monochromator. Features may be correlated with the Xe lamp spectrum and the filter changes indicated in Fig. 3, as well as with the photodiode quantum efficiency. The current agrees well with calculated current after understanding the UV drop.

When initially installed, the dark box was checked for light leaks with a Burle 8575 photomultiplier. The inevitable leaks were successively patched with black photographic tape until there was no difference between lights on/lights off behavior.

2.6. Dewar

The commercial dewar is attached to the dark box via a custom flange. Since the plywood does not provide enough dimensional stability for the demanding PSF measurements, it is also rigidly attached to the optical table.

A unique feature of the QE Machine is that the calibrated reference photodiode is inside the dewar, coplanar with the CCD. The CCD temperature is usually maintained at −140° C. The reference PD is mounted on an independent heat sink, and regulated to its calibration temperature, 25° C.

This arrangement means that except for the minor intensity corrections shown in Fig. 4, the CCD and PD are subject to exactly the same light intensity at the same time. Corrections for reflections from the quartz window are unnecessary.

Fig. 6 shows the current in this PD during early measurements. This is sufficient for noise in the picoammeter to be insignificant. However, for studies using long exposures at reduced intensity, this PD cannot be the primary reference. Instead, at higher intensity it is used to calibrate the PD at one of the small integrating sphere ports, which can then be used as the reference.

2.7. Controller and software

The CCD is controlled by a SDSU II Controller,[6] slightly modified to provide our large negative V_{dd} and the large ($\lesssim$ 100 V) bias needed to deplete the LBNL *p*-channel CCD's. The (linux) VOODOO program was modified, and a JAVA-based scripting capability was added.

A script controls the QE scan, steps through the requested wavelengths, and controls the shutters and monochromator, which in turn sets the appropriate filter position and light intensity (via the motorized slit widths). Typically, a scan goes from 300 nm to 1100 nm in 20 nm steps, then from 310 nm to 1090 nm in 20 nm steps. The `fits` images are then processed using IDL.

3. PERFORMANCE

Figure 7 shows preliminary results obtained with the Quantum Efficiency Machine. Reflectometer results, the subject of the next paper, are also shown. Given normalization and calibration issues not yet resolved for the QE measurements, the agreement is somewhat fortuitous. For comparison, the old results for a somewhat thicker

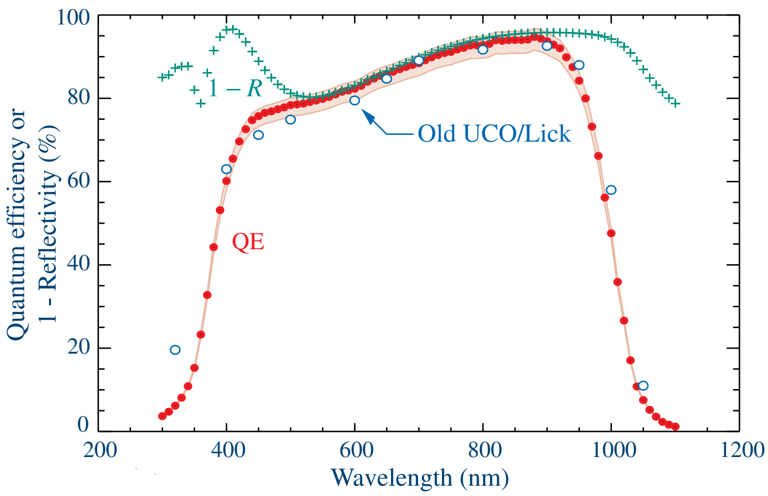

Figure 7. First results with The Quantum Efficiency Machine (solid circles and error band). $1 - R$ is also shown. Old UCO/Lick measurements are shown for comparison; that CCD had nominally the same antireflective coating but was thicker, so that the IR response is higher.

CCD with nominally the same antireflective (AR) coating are shown by the open circles. Results obtained with the CCD connected as a diode are consistent with the CCD-mode results.

Our $< 1\%$ error level goal means that most contributions must be far less than this. If a systematic error is one-sided, then the measurement is corrected by half this error so that there is not a systematic bias.

Most conceivable sources of error have been investigated and found to be negligible at this level: Filter out-of-bandpass leakage, 2nd order light from the monochromator, light leaks, noise in photodiode current measurements, picoammeter offset, and monochromator wavelength uncertainties. The dark current in a 1 cm^2 monitor diode in the integrating sphere is about 50 fA, so that neither light leakage nor PD noise is significant.

Intensity and hence exposure times, typically 5–10 s, are set by the requirement that the PD current should be well above noise in the picoammeter, which is less than 10^{-13} A. For longer exposures at reduced intensity, the monitor PD in the integrating sphere, calibrated using the standard PD, is used as the reference.

A normal scan consists of automatically repeating the following:

- The monochromator and (if called for) the filter wheel are moved to the new wavelength, after which there is a 500 s settling time.
- The motorized input and output slits are adjusted to obtain the desired intensity at the dewar.
- A 10 s dark is obtained with the large-aperture shutter closed.
- A 10 s exposure is obtained with the shutter open, at the end of which it closes.

Because the PD is coplanar with the CCD in the dewar, there are no geometrical or window-reflection corrections, except for the very tiny radial intensity variation shown in Fig. 4.

Fiducial areas are a different problem. So far it has been assumed that the PD area is exactly 1 cm^2, but this needs to be checked. Similarly, if the CCD is configured as a photodiode, a mask will be needed to define/check the fiducial area. So far we have simply taken the pixel area as correct, but there may be edge effects. Masks have been obtained but not yet installed.

The Uniblitz shutter remains open during the scan described above. The large-aperture shutter on which we presently depend is somewhat problematical. It takes 29 ms to open and 65 ns to close, which means that the center (the CCD fiducial area) and reference PD are illuminated for different times. Since aperture is star-shaped during the process, a correction is difficult to calculate. Better schemes are under discussion, and it will probably be moved to the light-entrance end of the dark box.

Finally, there is the problem of CCD gain calibration. The usual calibration is via ^{55}Mn K_α 5.90 keV x rays, assuming the traditional ∼3.65 eV/e-h conversion of energy deposit to collected charge at 300 K. Not only is this number uncertain at the 1% level, but it is temperature dependent. It is about 0.1 eV/e-h higher at our operating temperature. This problem is discussed in Appendix B.

Alternatively, the gain can be calibrated by the photon-transfer method[7, 8] or by comparing results between normal CCD readout (in ADU) with current when the CCD is connected as a photodiode. We use all three methods and get good agreement between gain from the fast photon-transfer analysis and the x ray calibration with the revised conversion factors, but comparisons are preliminary.

APPENDIX A. PARTS LIST

Table A1. Parts list. Excluded are the linux PC, the dewar, and the controller. The filters are listed in Table A2.

Item	Part number	Description
Xenon Light Source		
Lamp	Oriel 6257	100W Xenon Lamp
Socket adapter	Oriel 66150	Lamp Socket adapter
Lamp housing	Oriel 66902	50–500-W arc housing w. f/1 condenser
Power supply	Oriel 68907	Power supply for arc lamps
Lens holder	Oriel 6195	Lens holder for 1.5 lenses
f/4.6 focusing lens	Oriel 41575	152 mm UVFS lens
Stabilization	Oriel 68950	Light intensity controller system
Shutter	Uniblitz VS25S2ZM0R1	25 mm aperture shutter
Monochromator and filter wheel		
Monochromator	Oriel 77700	MS257 monochromator
Multiple grating Turret	Oriel 77708	Triple grating turret
Grating #1	Oriel 77742	1200/mm 350nm blaze
Grating #2	Oriel 77752	1200/mm 750nm blaze
Mirror	SP45700-1738	Mirror 50×50×6 mm, coated one side
Motor driven silt assembly (2 ea)	Oriel 77722	Variable input slit
Slit controller board (2 ea)	Oriel 77712	Motorized single slit control
Output Mirror	Oriel 77716	Motorized flip output mirror
Motorized Filter Wheel (2 ea)	Oriel 77737	
Fixed slit	Oriel 77212	3.16 mm fixed slit
Integrating Sphere	LabSphere CSTM US2000	20″ Integrating sphere
Light Measurement		
Photodiode	Hamamatsu S1337-1010BQ	Calibrated photodiode
Photodiode	Hamamatsu S2281	
Picoammeter (2 ea)	Keithley 6485	Picoammeters for PD readout
Optical Table	Newport IG-35-2	90×150 cm breadboard
	Newport IG-36-2	90×180 cm breadboard
Field shutter	Prontor* 100 mm	Shutter in front of dewar window

* Prontor was evidently bought by Zeiss, who no longer makes the shutter.

Table A2. Filters or pairs of filters used to make the ≈15-nm bandpasses shown in Fig. 3. The stack numbers refer to the bandpasses indicated in the figure.

	Stack	Part #	Type
Colored glass filters	1	Hoya U340	280 nm–370 nm
	2	Schott BG 28	380 nm–500 nm
Dielectric filters	3	LL-450-F	Long pass 450 nm
	3	LS-600-F	Short pass 600 nm
	4	LL-550-F	Long pass 550 nm
	4	LS-700-F	Short pass 700 nm
	5	LL-650-F	Long pass 650 nm
	5	LS-800-F	Short pass 800 nm
	6	LL-750-F	Long pass 750 nm
	6	LS-900-F	Short pass 900 nm
	7	LL-850-F	Long pass 850 nm
	7	LS-1000-F	Short pass 1000 nm
	8	LL-950-F	Long pass 950 nm

APPENDIX B. TEMPERATURE DEPENDENCE OF MEAN NUMBER OF e-h PAIRS PER eV OF X RAY ENERGY DEPOSIT

The conversion factor from ADU to *e-h* pairs in a CCD is commonly obtained using x rays of known energy from a calibration source such as the 5.90 keV ^{55}Mn K_α x ray from ^{55}Fe decay. Absolute QE is obviously dependent upon this number, so its systematic uncertainty is one of the many encountered in trying to make an absolute measurement of the QE. The factor is sometimes given as $w = 3.64$ eV/*e-h*, so that the scale factor is 5900/3.64 = 1620 *e-h* pairs. However, this is a room-temperature (300 K) value. The factor is dependent upon the silicon indirect bandgap energy, which increases significantly as the CCD is cooled. The room-temperature value is not correct for CCD's operated at 130–170 K. It is also energy-dependent, but is very nearly constant above several keV. There is evidence that it is different for α particles than for electrons or x(γ) rays; here we consider only the latter.

The conversion factor w has been measured for decades, usually at room temperature but sometimes at cryogenic temperatures. Dependable values with reasonable quoted errors at 300 K have usually been in the 3.62–3.68 eV/*e-h* range. 3.64 eV/*e-h* has frequently been reported in the older literature. ICRU 31[9] gives 3.68 ± 0.02 without references. In a recent paper Scholze et al. report 3.66 ± 0.03.[10] Since there is no way to sensibly decide how to weigh the many results, we tentatively adopt Scholze's value as a sensible middle ground. Given the other measurements, the error is more than likely closer to the ICRU estimate:

$$w(300\text{ K}) = 3.66 \pm (0.02 \text{ to } 0.03) \tag{1}$$

Both theoretically and experimentally, w can be represented by a linear function of the indirect bandgap energy,[11, 12]

$$w = a\,E_g + b\ . \tag{2}$$

Varshi[13] has proposed expressing the indirect bandgap energy E_g in silicon as a function of temperature T by*

$$E_g(T) = E_g(0) - \frac{\beta T^2}{T+\gamma}\ . \tag{3}$$

*This expression is a little more accessible in Refs. 14 and 15.

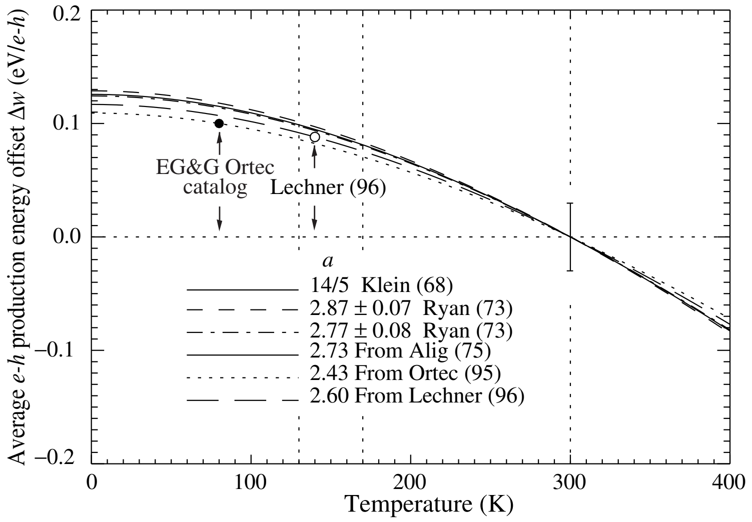

Figure 8. $\Delta w(T) = a[E_g(T) - E_g(300\text{ K})]$ for selected values of a for energetic photon and electron energy deposit in Si.

For silicon,

$$\begin{aligned} E_g(0) &= 1.1557 \text{ eV} \\ \beta &= 7.021 \times 10^{-4} \text{ eV/K} \\ \gamma &= 1108 \text{ K} . \end{aligned} \tag{4}$$

With these constants, $E_g(300\text{ K}) = 1.1108$ eV. Many values very close to this, for example 1.12 eV (commonly) and 1.107 eV (Handbook of Chemistry and Physics) can be found.

It is convenient to rewrite Eq. 2 as

$$\Delta w(T) = w(T) - w(300\text{ K}) = a\left[E_g(T) - E_g(300\text{ K})\right] . \tag{5}$$

This separates the temperature dependence problem from that of finding w at 300 K.

Published results for the temperature dependence, reduced to Δw, are shown in Fig. 8. Ryan[16] reports $w =$ 3.631 eV/e-h at 300 K and 3.745 at 100 K. The EG&G Ortec catalog[17] gives 3.62 at room temperature and 3.72 at 80 K. In more recent careful experiments, Lechner and Strüder[18] report $w(E_x, 140\text{ K})/w(E_x, 300\text{ K}) = 1.024$. We use these single values and Eq. 5 to draw the complete curves. In the other cases, values of a are reported. The agreement is remarkable; the uncertainty in Δw at the usual CCD operating temperatures is about 0.01. We find $\Delta w = 0.098$ at 130 K an 0.080 at 170 K. However, the shift changes w by as much as 2.7%.

In summary: For an average photon in the 5.90 keV ^{55}Mn K$_\alpha$ x ray peak, we expect 1570 ± 13 e-h pairs in a CCD at 140 K rather than the traditional 1620 e-h pairs.

For the CCD now being used to debug the system, operating at −140 K, we have obtained a gain of 1.473 ± 0.003 via the fast photon transfer method.[7,8] Under the same conditions we observe a mean of 2330 counts for the 5.90 keV ^{55}Mn K$_\alpha$ x ray. Using the photon-transfer method gain, we find $w = 1.473 \times 5900/2330 = 3.73$ eV/e-h. The agreement with the 3.76 ± 0.02 obtained above is probably fortuitous at this point, but it appears that this route offers an alternate way to evaluate w.

ACKNOWLEDGMENTS

This work was supported by the Director, Office of Science, of the U.S. Department of Energy under Contract No. DE-AC02-05CH11231 We have profited greatly in the design and construction of The Quantum Machine from papers and discussions with P. Amico,[5] D. Guzman,[19] M. Lesser,,[20] S. Miyazaki,[21] R. Stover, the Indiana/Michigan group, and others who have built similar instruments.

REFERENCES

1. S. E. Holland et al., IEEE Trans. Electron Dev. **50** (3), 225–238 (January 2003).
2. J. Steckert, *Design, implementation, and setup of an automated quantum efficiency measurement system for charge-coupled devices*, FH Karlsruhe (2005) (Unpublished diplom thesis).
3. SNAP Collaboration, "Supenova/ Acceleration Probe: A satellite experiment to study the nature of the dark energy," `astro-ph/0405232` (submitted to Proc. Astron. Soc. Pacific)
4. M. Fabricus et al., SPIE **6068**, (2006). (Proc. Symp. on Electronic Imaging, 15–19 January, 2006, San Jose, CA.)
5. P. Amico and T. Bohm, "The ESO CCD testbench," `http://www.eso.org/projects/odt/CCDtestbench/Testbench.html.`
6. R. Leach, F. Beale, and James Eriksen, "New Generation CCD Controller Requirements and an Example: The San Diego State University Generation II Controller," Proc. SPIE **3355**, 512 (1998) (Kona).
7. J. R. Janesick, *Scientific charge-coupled devices*, SPIE Press, Bellingham, WA (2001)
8. F. Christen et al., "Fast conversion factor (gain) measurement of a CCD using images with vertical gradient," Scientific Detectors Workshop, Catania, Sicily (2005).
9. ICRU Report 31, "Average Energy Required to Produce an Ion Pair," (1979)
10. F. Scholze, H. Rabus, & G. Ulm, J. App. Phys. **84**, 2926–2939 (1998); F. Scholze, H. Henneken, P. Kuschnerus, H. Rabus, & G. Ulm, Nucl. Instrum. Methods **A439**, 208–215 (2000);
11. C. A. Klein, J. Appl. Phys. **39**, 2029 (1968)
12. R. C. Alig, S. Bloom, & C. W. Struck, Phys. Rev. **B22**, 5565–5582 (1980)
13. Y. P. Varshni, Physica **34**, 149 (1967)
14. K. Rajkanan, R. Singh, & J. Schewchun, Solid-State Elec. 22, 793–795, (1979)
15. S. M. Sze, *Physics of Semiconductor Devices*, John Wiley & Sons, (1969)
16. R. D. Ryan, IEEE Trans. Nucl. Sci. **NS-20**, no. 1, 473–480, Feb. 1973
17. EG&G Ortec, "Modular Pulse-Processing Electronics and Semiconductor Radiation Detectors," #95 (November 1994)
18. P. Lechner & L. Strüder, Nucl. Instrum. Methods **A354**, 464 (1995).
19. D. Guzman, S. Blais-Oullette, M. Bonati, and A. Elgamil, "A versatile wavelength-dependent spectrophotometer for efficiency measurements of CCD and cryogenic gratings," Proc. SPIE **5499**, 371 (2004) (Glasgow).
20. M. P. Lesser and B. L. McCarthy, "Quantum Efficiency Characterization of Back Illuminated CCDs," Proc. SPIE **2654b**, 278 (1996).
21. S. Miyazaki et al., "Characterization and mosaicing of CCDs and applications to the Subaru wide field camera (Suprime-Cam), Proc. SPIE **3355** (1998) (Kona); S. Myazaki, "CCD Characterization," `http://anela.mtk.nao.ac.jp/detectorlab/qebench.htm`